Piezo-spectroscopic assessment of nanoscopic residual stresses in Er^{3+}-doped optical fibres

2003 J. Phys.: Condens. Matter 15 7687

(http://iopscience.iop.org/0953-8984/15/45/008)

INSTITUTE OF PHYSICS PUBLISHING JOURNAL OF PHYSICS: CONDENSED MATTER

J. Phys.: Condens. Matter **15** (2003) 7687–7695 PII: S0953-8984(03)62981-4

Piezo-spectroscopic assessment of nanoscopic residual stresses in Er^{3+}-doped optical fibres

Giuseppe Pezzotti[1,4], **Andrea Leto**[1], **Katsuhisa Tanaka**[2] **and Orfeo Sbaizero**[3]

[1] Ceramic Physics Laboratory and Research Institute for Nanoscience, RIN, Kyoto Institute of Technology, Sakyo-ku, Matsugasaki, 606-8585 Kyoto, Japan
[2] Department of Chemistry and Materials Technology, Kyoto Institute of Technology, Sakyo-ku, Matsugasaki, 606-8585 Kyoto, Japan
[3] Materials Engineering and Applied Chemistry Department, University of Trieste, 34127 Trieste, Italy

Received 30 April 2003
Published 31 October 2003
Online at stacks.iop.org/JPhysCM/15/7687

Abstract

A quantitative characterization of residual stresses was performed with a nanometric spatial resolution in Er/Ge-doped silica glass fibres. Stresses were assessed by a piezo-spectroscopic technique (i.e., monitoring wavelength shifts), which used the electro-stimulated luminescence of optically active defects in silica glass. Residual stresses of GPa magnitude were found near the core/cladding interface by using a nanometre-sized electron probe. Diffusion of Er/Ge ions from the core towards the cladding area was clearly observed in this optical device and the occurrence of this diffusive phenomenon permitted stress measurement in extended cladding regions beyond the core/cladding interface. A discussion is given of the impact of residual stresses on the optical performance of the fibre device.

(Some figures in this article are in colour only in the electronic version)

1. Introduction

Optical fibre devices include two concentric glass components, the inner core and the outer cladding, and a buffer coating material that insulates the core and cladding from the environment. The buffer coating also helps the fibre retain its intrinsic strength. The inner core is intentionally doped to achieve a refractive index higher than the outer cladding, so that a light ray injected into the core at an angle greater than a critical angle will eventually hit the core/cladding interface but be reflected back into the core with minimum signal loss [1]. Optically active, trivalent rare earth ions result in significantly shorter gain lengths than can be fabricated in glasses traditionally used for fibres. In this context, Er^{3+}-doped fibres are

[4] Author to whom any correspondence should be addressed.

typically manufactured from fused silica due to their unique ability to transmit optical signals over long distances with relatively low attenuation. These combined aspects of the Er^{3+}-doped silica glass and reported gain characteristics support it as a prime candidate for compact, high performance, and cost effective optical fibre devices [2].

Residual stress in glass fibres can affect the optical properties of the fibres with respect to two main aspects:

(i) the refractive index can be changed by residual stress through the stress-optic effect [3]; and
(ii) optical loss can be increased by residual stress-induced Rayleigh scattering and structural imperfections [4].

Residual stress in the fibres results mainly from a superposition of a thermal stress field, caused by a difference in thermal expansion coefficients between core and cladding, and a mechanical stress field, induced by a difference in viscosity between the two regions [5]. Unlike chemical and microstructural characterizations [6], micromechanical characterizations have not yet been fully attempted and no quantitative experimental result has been systematically reported to directly support the relationship between internal (residual) stress distribution and fibre optical performance. In this paper, we investigated the residual stress field developed during processing on the optical fibre section by the direct measurement of wavelength shifts of the electron-stimulated luminescence spectrum of silica. We have recently developed a cathodoluminescence spectral analysis based on wavelength shift and applied this spectral peak-shift method (luminescence piezo-spectroscopy) to the measurement of nano-scale internal stresses in amorphous solids [7, 8]. This method is based on the presence (or, eventually, the intentional incorporation) of an atomic trivalent rare earth ion as a 'atomic-scale stress sensor' into the glass network, followed by a quantitative evaluation of the shift of the light spectrum emitted upon irradiation by the electron beam with and without an applied (or residual) stress. In this paper, we show for the first time that the intrinsic luminescence arising from oxygen-related defects of the silica network can also be used for stress assessments. Electron-stimulated luminescence experiments have so far been performed in aluminosilicate glass, fluorophosphate, borosilicate and high-silica glasses, with Sm^{3+}, Nd^{3+} or Er^{3+} as dopants. The majority of those investigated glasses are materials actually used in hard-disk packages and optical fibre technology.

2. Experimental procedures

The Er^{3+}-doped/high-silica optical fibre investigated in this study was a core/cladding structure obtained from Mitsubishi Cable, Ltd. The core of the fibre (diameter $2R_c = 4.8\ \mu$m) contained 560 ppm Er_2O_3, 500 ppm Al_2O_3, and 13.7 mol% GeO_2. The clad (diameter $2R_{cl} = 120\ \mu$m) was a high-silica glass grade. However, the precise composition of the optical fibre, including the complete table of trace dopant and impurities, was covered by industrial secret and not available to the authors. A portion of fibre about 5 mm in length was cut perpendicular to the fibre axis and embedded into epoxy resin for easier handling. The fibre section was then ground and polished with successively finer diamond pastes until optically flat surfaces were produced. Finally, a light ion milling procedure was applied at low angles in order to minimize the effect on the residual stress field of the machining procedure. The scanning electron microscope (SEM) employed in this study was a new thermal filament type field emission gun (FEG) device with a lateral spatial resolution of 1.5 nm (JSM-6500F, JEOL, Tokyo, Japan). The microscope was mounted within a cut-out on an air-suspended optical table, thus eliminating vibration noises and aiding optical alignment. A high-sensitivity cathodoluminescence detector unit

(MP-32FE, Atago Bussan, Horiba Group, Tokyo, Japan) was employed for the collection of light upon reflection into an ellipsoidal mirror and transmission through an optical fibre. The emitted light spectrum was analysed using a triple-monochromator equipped with a CCD camera. A new mapping device (PMT R943-02 Select, Atago Bussan, Horiba Group, Tokyo, Japan) and related software was developed, which enabled us to automatically collect arrays of spectra with nanometric spatial resolution and to simultaneously analyse a large number of spectra in real time with spectroscopic data acquisition. A low accelerating voltage (typically 1.0 kV) and high filament current (about 80 μA) was used throughout the piezo-spectroscopic experiments to inject electrons into the surface with minimal lateral scattering. A good quality luminescence spectrum of silica, suitable for precise mathematical fitting, could be collected within a few seconds of accumulation time. It should be noted that the efficiency of the spectrum depends considerably on the dopant concentration and on the concurrent presence of other impurities (co-dopants). Although the relative efficiency of luminescence in a specific host is essentially site-independent [9], the presence of co-dopants may affect the stress-free wavelength of the emission. Therefore, case-by-case spectral calibrations should be performed even for glasses, which nominally contain the same luminescent probe.

Including the occurrence of electron beam broadening, a high spatial resolution (better than 5 nm) could be achieved in the present study, as calculated according to the modified Grün equation [10]. An experimental assessment of the spatial resolution into the FEG-SEM, using an interface between alumina and the Er^{3+}-doped-glass, suggested a broadening magnitude of $<$3 nm in diameter, thus supporting the above theoretical assessment.

As for the stress calibration, a laboratory-made bending micro-jig was equipped with a load cell of 100 N and placed into the electron microscope. A small bar, machined from the fibre preform, was loaded in the miniature bending jig. Luminescence spectra were recorded as a function of the externally applied load. Tensile or compressive stresses were calculated from the externally applied load, according to the elastic beam theory. In the relatively short time necessary for collecting fluorescence spectra in the present experiments, no significant relaxation of the applied load could be detected. A complete description of both loading jig and calibration procedure is given in [7] and [8]. In the investigated stress interval, the relationship between stress and spectral shift obeyed a linear equation, as follows:

$$\sigma_u = \Delta\lambda/\Pi_u \tag{1}$$

where Π_u is referred to as the piezo-spectroscopic coefficient for uniaxial stress. An average hydrostatic (three-dimensional) piezo-spectroscopic coefficient was taken as $\Pi_h = 3\Pi_u$, and used for calculating residual hydrostatic stresses, σ_h. This choice of Π_h assumes a three-dimensionally homogeneous and isotropic structure for the glass. Since residual (thermal) stresses, resulting from sample processing, were the object of our investigation, a stress-free (reference) wavelength, λ_0, had to be carefully selected. For this purpose, a map of luminescence spectra was collected within the sample from a small piece of core material cut out from the cladding and finely crushed, thus having (nearly) zero residual stress and no externally applied stress. The band position associated with an average of 5×10^3 randomly collected spectra was taken as the reference stress-free band position, λ_0. A similar procedure was adopted for determining the λ_0 of the cladding glass.

3. Results and discussion

Typical electron-stimulated luminescence spectra from the fibre device are shown in figures 1(A) and (B), which were collected from the filamentary Er/Ge-doped core and the high-silica cladding regions of the fibre, respectively. The luminescence spectrum in the core

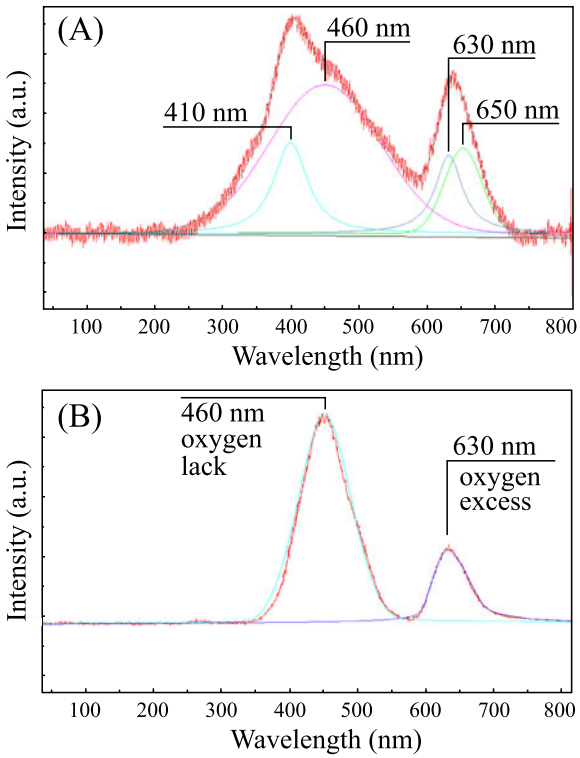

Figure 1. Typical electro-stimulated luminescence spectra taken from core (A) and clad (B) areas of the Er^{3+}-doped optical fibre device.

region (figure 1(A)) appears to arise from the overlapping of four bands, two bands located at 410 and 650 nm and two additional bands located at 460 and 630 nm. The electro-stimulated luminescence band located at 410 nm arises from dicoordinated Ge [11]. The additional two bands at 460 and 630 nm were reported to yield from lack and excess of oxygen in the silica structure, respectively [11, 12]. In particular, the intrinsic defects related to lack and excess of oxygen, which dominate the visible part of the optical spectrum of vitreous silica, seem to be peculiar to the glassy state only. They can be observed in quartz only after irradiation by fast particles, usually neutrons, capable of creating amorphized microregions and microvoids within the crystalline structure [11]. An indirect confirmation that the two observed bands actually arose from the high-silica vitreous structure could be obtained from examining the spectral characteristics of the cladding area (figure 1(B)), which indeed systematically showed only two bands located at 460 and 630 nm. All the detected luminescence bands showed a linear wavelength dependence on stress. However, given the strong band overlapping in the core structure, a reliable band-shift assessment could be obtained only for the band located at 410 nm. The stress assessment was made possible by the spectrum deconvolution treatment shown in figure 1(A). Band assignment was based principally on data from bulk undoped and Er/Ge-doped silica materials. The deconvolution into two or three bands did not provide a good fit between the experimental spectra and the sum of the Gaussian/Lorentzian peaks. The addition of a fourth peak improved the results and led to a reproducible unique solution. A confirmation of the correctness of the selected deconvolution treatment could be obtained by taking advantage of the rather high increase in relative intensity of the 410 nm

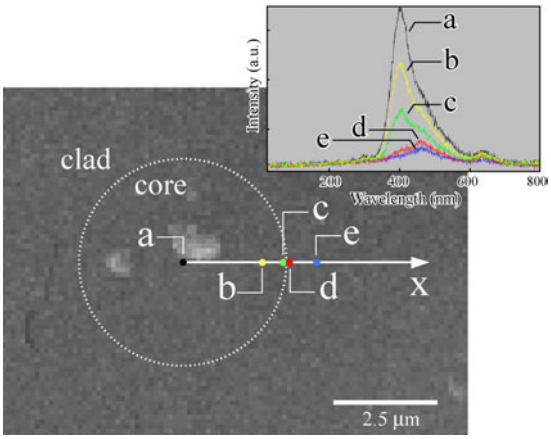

Figure 2. High-resolution scanning electron micrograph of the core area (encircled area). The variation of the electro-stimulated luminescence spectrum is also shown from the centre of the core towards the clad of the Er^{3+}-doped optical fibre device.

Table 1. Piezo-spectroscopic coefficients and standard deviation of various investigated electro-stimulated luminescence peaks.

Band (nm)	Π_u (nm GPa^{-1})	$\pm\Delta\Pi$ (nm GPa^{-1})	Origin
410	6.744	5.5×10^{-3}	Dicoordinated Ge
460	−6.529	1.37×10^{-3}	Silica oxygen lack
630	7.137	3.122×10^{-3}	Silica oxygen excess

band (i.e., above the 460 nm band) upon increasing acceleration voltage. It should also be noted that in a bending configuration, the stress state is constant along an axis perpendicular to the side surface of the tested bar. Therefore, an increase in acceleration voltage, which is usually accompanied by an increase in penetration depth, should not involve any variation in the probed stress field. Table 1 summarizes the results of piezo-spectroscopic calibrations with respect to all the available luminescence bands. An evaluation of the stress sensitivity of each band is given in terms of the slope, Π_u, of a plot of uniaxial stress, σ_u, versus spectral shift, $\Delta\lambda$ (cf equation (1)). The high confidence of the present stress measurement is represented in the relatively low scattering, $\Delta\Pi$, of the piezo-spectroscopic coefficient, Π_u, as explicitly shown in table 1.

Figure 2 shows the change in spectrum profile from the centre of the core towards the clad, with the sudden disappearance of the 410 nm band nearby the core/cladding interface. Given the good sensitivity of the 410 nm band to stress, this band was selected for residual stress assessments within the fibre core. Both bands belonging to lack of and excess oxygen in the high-silica clad reliably shifted upon stress application with respect to their respective (unstressed) positions, λ_0, the shift rates being of a magnitude comparable with that of the 410 nm band (cf table 1). In assessing residual stresses in the clad structure, the band lacking oxygen centred at 460 nm was selected because of its relatively high intensity.

Figure 3 shows an SEM micrograph of the cross section in the Er^{3+}-doped fibre. A band intensity map and a residual stress map are shown as insets, as collected at the core/clad interface using the luminescence band located at 410 nm. The spatial resolution of this stress measurement was better than 5 nm. The stress map clearly indicates a region of relatively high

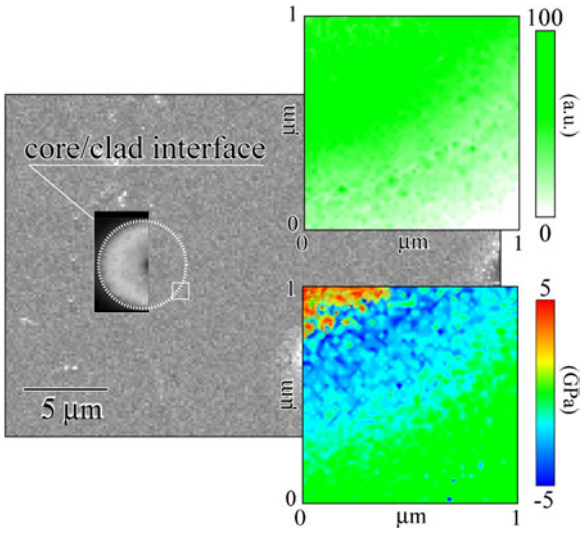

Figure 3. The assessment of electro-stimulated luminescence spectra on the section of the optical fibre device. The circle drawn on the SEM micrograph locates the fibre core. The core is not visible by conventional scanning electron imaging (right side of the circle) but it can be visualized by mapping the intensity of the luminescence spectrum as displayed in the left side of the circle. High-resolution intensity and residual stress maps collected nearby the core/clad interface (square area on the SEM micrograph) are shown in insets. The minus sign in front of stress values represents a compressive stress.

tensile stress that corresponds to the core area, whilst in the clad region a compressive-stress region was found in the neighbourhood of the core/clad interface. It should be noted that the 410 nm band was generally not detectable in the clad area; however, the stress at the core/clad interface could be measured by virtue of a certain amount of Ge ions, which diffused during processing from the core area towards the clad (cf intensity map in inset of figure 3). The diffusive area was about 0.5 μm in thickness. The compressive stress developed within the intermediate (diffusive) region, in which Er and Ge were present into silica, counterbalances the residual tensile stress developed in the core. It should be noted that both diffusion and stress trends shown in figure 3 were general and could be also confirmed at different locations of the core/clad interfaces. The maximum stress magnitude recorded with a nanometric spatial resolution was of GPa order; however, the stress distribution was highly inhomogeneous. The detected inhomogeneous (micellar) structure was similar to that observed in a previous work on Sm^{3+}-doped glass samples [7]. From a general point of view, the way nanometre-scale stresses distribute within the glass structure may prove either the presence of nanocracks or the coexistence of strong and weak interpenetrating networks, with the attendant appearance of cohesive molecular groupings which mutually interact via the weak network while being internally bound throughout the strong. This feature in the residual stress distribution has been discussed in some detail in two previously published papers [7, 8].

Figure 4 shows a high-resolution SEM micrograph of an area in the clad (A) selected from an area far away from the core/clad interface; a map, collected at the same location, of the intensity of the band at 460 nm (B); and a hydrostatic stress map (as calculated from the shift of the 460 nm band with a $\Pi_h = 3\Pi_u$ value according to table 1) (C). The spatial resolution of the stress measurement here was better than 10 nm. The band intensity map showed low intensity in cracked areas. As suggested by a comparison between (A), (B) and (C), local

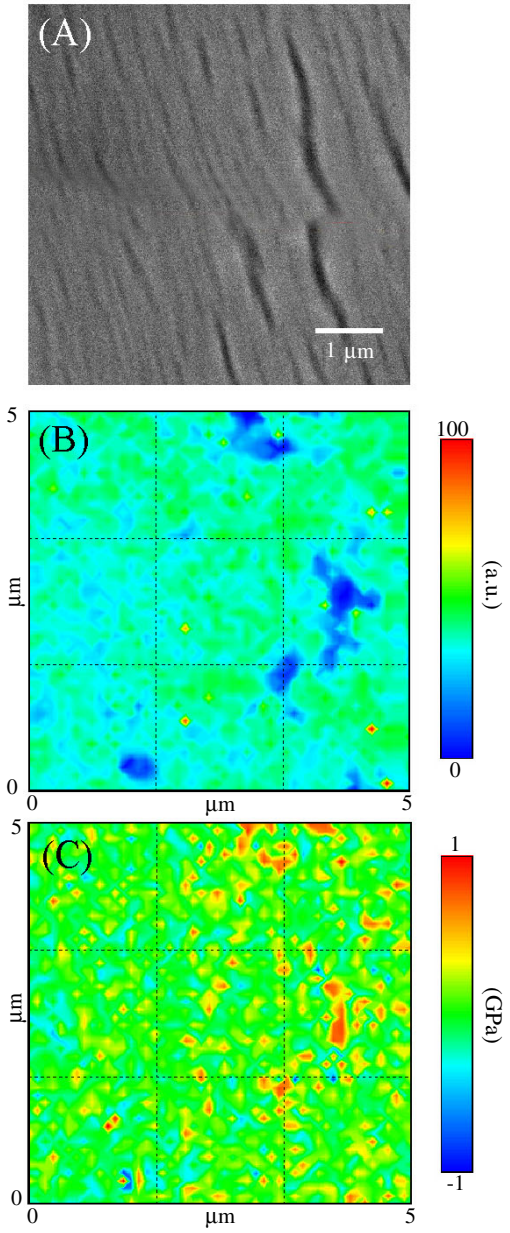

Figure 4. SEM image of microcracks in the clad region (A) and related intensity (B) and stress (C) maps probed by means of the 460 nm silica band.

accumulation of tensile stress was due to the presence of nanocracks within the clad structure. The tensile stress intensification noticed in correspondence of the nanocracks may lead to remarkable degradation of mechanical strength in the fibre device. However, some areas of residual compressive stress were also found and the average surface residual stress field in areas far away from the core/clad interface was almost zero, showing that basically the presence of nanocracks has released the residual stress stored in the cladding area. It should be noted that,

as mentioned in discussing the stress map in figure 3, nanocracks were present both in the core and cladding areas of the present fibre device. The important difference between these two regions is that, in areas (from the cladding side) far away from the core/cladding interface, the formation of nanocracks has mainly released residual stresses from the drawing process; on the other hand, despite the formation of nanocracks, residual stresses of significant magnitude remain stored nearby the core/cladding interface.

The results of nanomechanics characterizations suggest a significant impact of nanocracking, as developed during fibre processing, on the mechanical strength of the clad, and a remarkable effect of the residual stress field at the core/clad interface. This latter effect should strongly affect the optical performance of the fibre device. The residual stress contribution to the refractive index can be quantitatively characterized by tensorial stress-optical equations. However, for light propagating along a homogeneous and isotropic medium, the change in refractive index, Δn, in the radial direction of the fibre (due to residual stress) can be expressed by the following linear relationship [13]:

$$\Delta n = C\sigma_{\mathrm{h}}/3 \tag{2}$$

where C is the stress-optic coefficient (e.g., -4.2×10^{-12} Pa^{-1} for pure silica glass [3]) and σ_{h} is the average hydrostatic residual stress ($\sigma_{\mathrm{u}} = \sigma_{\mathrm{h}}/3 =$ uniaxial stress). Given the negative value of C for silica glass, it follows that a residual compressive stress (i.e., for convention with a negative sign) stored in the clad of the fibre will produce an increase in the refractive index of the fibre clad. According to similar considerations, a tensile residual stress will decrease the refractive index of the core. According to Snell's law [13], the higher the refractive index of the core with respect to that of the clad, the lower the signal loss in the glass fibre. Therefore, two contributions to the refractive index of the optical fibre, Δn_{c} and Δn_{cl}, should be considered: one arising from the tensile and the other from the compressive (residual) stress field, which develop in the neighbourhood of the core/clad interface from the core and the clad side, respectively (cf figure 3). According to equation (1), $\Delta n_{\mathrm{c}} < 0$ and $\Delta n_{\mathrm{cl}} > 0$, thus the intrinsic mismatch between the refractive indexes of core and clad, Δn_{i}, can be significantly reduced to a lower (real) value, Δn_{r}, by virtue of residual stresses:

$$\Delta n_{\mathrm{r}} = \Delta n_{\mathrm{i}} - (\Delta n_{\mathrm{cl}} - \Delta n_{\mathrm{c}}). \tag{3}$$

It should be noted that, given the local impact of stress on signal loss, residual stress intensification at the core/clad interface may involve a higher signal loss as compared to that predictable from residual stress values averaged over the entire core and clad regions (i.e., as calculated from thermal expansion mismatch between core and clad by means of elastic mechanics theory [14], experimentally collected along the fibre axis with neglecting the stress distribution along the fibre section [15], and/or experimentally collected with a low spatial resolution). This concept can be rigorously expressed in a mathematical form by estimating the difference between the $(\Delta n_{\mathrm{i}} - \Delta n_{\mathrm{r}})$ values calculated with and without considering the stress intensification at the core/clad interface. When such a stress intensification is taken into account and a system of cylindrical coordinates, r, θ and z, is established with the origin on the fibre axis, we can place

$$\Delta n_{\mathrm{cl}} = \frac{1}{\Delta\theta} \sum_{j=0}^{p} \int_{\theta_j}^{\theta_{j+1}} C\sigma_{\mathrm{u}}^{(\mathrm{cl})}(\theta_j)\,\mathrm{d}\theta \tag{4}$$

$$\Delta n_{\mathrm{c}} = \frac{1}{\Delta\theta} \sum_{k=0}^{q} \int_{\theta_k}^{\theta_{k+1}} C\sigma_{\mathrm{u}}^{(\mathrm{c})}(\theta_k)\,\mathrm{d}\theta \tag{5}$$

with $j = 0, 1, 2, \ldots, p$ and $k = 0, 1, 2, \ldots, q$, where p and q are number of circular sectors at the core/clad interface for which stress measurements were performed from the clad and

the core side, respectively; $\sigma_u^{(c)}$ is one third of the (average) hydrostatic residual stress $\sigma_h^{(c)}$ measured by piezo-spectroscopy in the core region along the radial interval $R_c - s < r < R_c$ and $\sigma_u^{(cl)}$ is one third of the (average) hydrostatic residual stress $\sigma_h^{(cl)}$ measured by piezo-spectroscopy in the clad region along the radial interval $R_c < r < R_c + s$. Both $\sigma_u^{(c)}$ and $\sigma_u^{(cl)}$ are functions of the angular coordinate θ; s is the spatial resolution of the stress measurement (i.e., $\sim$3 nm) and $\theta_{j+1} - \theta_j = \Delta\theta = 2s/R_c$. On the other hand, a calculation which neglects residual stress intensification at the core/clad interface is simply based on equation (2) with the assumption that σ_h is equal to the average residual stress in the core region. Note that in this latter case the contribution, Δn_{cl}, to the refractive index mismatch between core and clad is negligible because the residual stress averaged over the entire clad area is of a negligible magnitude. According to equation (3) and obtaining Δn_c and Δn_{cl} from a numerical integration of equations (4) and (5) (i.e., using experimental stress data from figure 3), for example, we calculate $\Delta n_i - \Delta n_r = 4.8 \times 10^{-3}$ versus a value 6.4×10^{-4} obtained by neglecting the residual stress intensification at the core/clad interface.

4. Conclusion

From the present nanomechanics assessments, it can be concluded that the manufacturing process of Er^{3+}-doped optical fibres has to be accurately designed to avoid piling up of tensile residual stresses within the narrow core region. Such a tensile stress field is counterbalanced by a compressive stress field stored within the clad area adjacent to the core/clad interface, which duplicates the negative effect on signal loss. High-resolution piezo-spectroscopic stress assessments provide a quantitative estimate of the residual stress intensification at the core/clad interface. This can in turn allow the reliable assessment of the actual mismatch between the refractive indexes of fibre core and clad. In conclusion, we have shown here that electron-stimulated piezo-spectroscopy is a unique tool for the quantification of stress information on a nanometre scale within glasses. A peculiarity is revealed in the micellar structure found in the present luminescence assessment (both for band intensity and shift), which may reflect the presence of nanocracks or the existence of a nanometre-scale meso-structure in the present high-silica glass. The obtainment of physical insight into the mechanics of nanometre-scale glass structures can lead to an improved design and to a better control of the performance of future optical devices.

References

[1] Miniscalco W J 1993 *Rare Earth Doped Fiber Lasers and Amplifiers* ed M J F Digonnet (New York: Dekker) pp 19–133
[2] Simpson R 1993 *Rare Earth Doped Fiber Lasers and Amplifiers* ed M J F Digonnet (New York: Dekker) pp 1–18
[3] Hermann W, Hutjens M and Wiechert D U 1989 *Appl. Opt.* **28** 1980
[4] Primak W and Post D 1959 *J. Appl. Phys.* **58** 779
[5] Paek U C and Kurkjian C R 1975 *J. Am. Ceram. Soc.* **58** 330
[6] Wyatt R 1989 *Proc. SPIE* **1171** 54
[7] Pezzotti G 2003 *Microsc. Anal.* **33** 5
[8] Pezzotti G 2003 *JEOL News* **38** 13
[9] Hufner S 1978 *Optical Spectra of Transparent Rare-Earth Compounds* (New York: Academic)
[10] Everhart T E and Hoff P H 1971 *J. Appl. Phys.* **42** 5837
[11] Skuja L 1998 *J. Non-Cryst. Solids* **239** 16
[12] Sakurai Y and Nagasawa K 2000 *J. Appl. Phys.* **88** 168
[13] Born M and Wolf E 1965 *Principles of Optics* (New York: Pergamon)
[14] Krohn D A 1970 *J. Am. Ceram. Soc.* **53** 505
[15] Kim B H, Park Y, Ahn T-J, Kim D Y, Lee B H, Chung Y, Paek U C and Han W T 2001 *Opt. Lett.* **26** 1657